

Soft Phonon Mode Dynamics and Phase Transitions in Aurivillius Type Structures

Deepam Maurya¹, Fu-Chang Sun², Deepu George³, Sanjeev K. Nayak², Abhijit Pramanick⁴,
Min-Gyu Kang¹, Hyun-Cheol Song¹, Ali Charkhesht³, S. Pamir Alpay^{2*}, Giti A.
Khodaparast³, N. Q. Vinh^{3*}, and Shashank Priya^{1*}

¹*Bio-inspired Materials and Devices Laboratory (BMDL), Center for Energy Harvesting
Materials and Systems (CEHMS), Virginia Tech, 24061 USA*

²*Department of Materials Science & Engineering, Department of Physics, Institute of Materials
Science, University of Connecticut, Storrs, CT 06269-3136, USA*

³*Department of Physics, Virginia Tech, 24061 USA*

⁴*Department of Physics and Materials Science, City University of Hong Kong, Kowloon, Hong
Kong SAR*

We report the dynamics of soft phonon modes and their role in the structural phase transitions of the Aurivillius materials studied by employing terahertz frequency-domain spectroscopy, atomic pair distribution function analysis, and first-principles calculations. We have chosen $\text{Bi}_4\text{Ti}_3\text{O}_{12}$ as a model system and discovered soft phonon modes associated with the paraelectric tetragonal to the ferroelectric monoclinic structural transformations. The displacement of Bi results in polarization variations in Bi layered materials, and the anharmonicity in Bi–O bonds plays a significant role in phonon softening and the structural phase transition.

PACS numbers: 78.30.-j, 63.20.-e, 77.80.B-, 77.80.-e

* Corresponding authors: spriya@vt.edu, vinh@vt.edu, pamir.alpay@uconn.edu

The knowledge of soft phonon mode properties is crucial for understanding the origin of lattice instabilities and structural phase transitions in bismuth layered ferroelectrics (Aurivillius-type structures). Typically, the structural phase transitions in these materials occur with the heavily damped phonons in the terahertz (THz) frequencies [1,2]. Understanding dynamics of these phonon modes are critical for designing high performance ferroelectric materials [3]. The number of phonon modes are defined by the nature of the symmetry change during the transition. The phase transition involving more than one soft phonon modes [4] and corresponding order parameters may induce intermediate phase transitions. However, the condensation of more than one phonon modes at a single transition is quite unusual [5]. Here, we used $\text{Bi}_4\text{Ti}_3\text{O}_{12}$ (BiT) as a model system to understand the phonon modes related to the structural phase transitions in Aurivillius materials. Using a unique high sensitivity and high resolution THz frequency-domain spectroscopy, we have experimentally discovered, so far elusive, three phonon modes related to the symmetry breaking from high temperature tetragonal to low temperature monoclinic phase in BiT. We have further employed atomic pair distribution function (PDF) analysis to correlate the dynamics of the Bi ions with the phonon dynamics. These results are complemented by First-principles calculations for temperature dependent phonon computations, which describe the THz spectroscopy and identify that the main contribution to the atom-projected phonon density of states (DOS) comes from Bi atoms.

Aurivillius structures (Bi-layered structure) $\text{Bi}_2\text{A}_{n-1}\text{B}_n\text{O}_{3n+3}$ ($n = 1-6$) have recently attracted great attention due to the important ferroelectric, dielectric, and piezoelectric properties along with high Curie temperature ($>600^\circ\text{C}$)[6]. The ferroelectric members of this family have potential applications in high temperature sensors and fatigue-free ferroelectric memory devices etc. [7]. Furthermore, these layered materials exhibit anisotropic and very low thermal conductivity due to

effective phonon scattering from their layered structure [8]. The structure of this class of materials, consists of perovskite-like block $(A_{n-1}B_nO_{3n+1})^{2-}$ interleaved with fluorite like $(Bi_2O_3)^{2+}$ layers perpendicular to pseudo-tetragonal c -axis [9]. Out of various other members of the Aurivillius family, $Bi_4Ti_3O_{12}$ -based material systems exhibit relatively higher polarization [10]. Recent interest in 2D materials has raised additional interest in layered structures due to the possibility of synthesizing nanosheets through exfoliation process. In terms of phase transformations characteristics, BiT undergoes a ferroelectric phase transformation from the high temperature tetragonal paraelectric phase to a lower temperature polar monoclinic phase without any intermediate transitions [11] that are common in prototypical perovskite ferroelectrics such as $BaTiO_3$.

Much effort has been devoted to understand structural changes with respect to temperature in Aurivillius ferroelectric materials. Theoretical [5] and experimental [12] studies have reported possible triggered phase transition from low temperature polar monoclinic phase to high temperature tetragonal phase of BiT. The low temperature ferroelectric monoclinic phase of BiT requires condensation of at least three different symmetry breaking modes, which have hitherto not been observed experimentally [5]. An observation of the temperature dependence of the lowest frequency polar phonon mode (denoted as a soft phonon mode), using Raman scattering is not very convincing, because, the intensity of the soft phonon mode decreases rapidly with increasing temperature [4].

Here, we employ a THz frequency-domain technique to detect the optical phonons where large contribution of dielectric polarization is found along the plane perpendicular to the stacking direction in the BiT ferroelectric ceramics. In previous studies, the dynamics of the ferroelectric transition in Bi-layered ferroelectric materials have been investigated using the THz time-domain

spectroscopy [4,13], where only one optical soft mode was observed in the ferroelectric phase of the BiT material [4], which was underdamped above T_c due to the change of selection rules in the paraelectric phase. However, using our high resolution and large dynamic range THz frequency-domain spectroscopy [14], we have observed multiple optical modes which could explain the phase transition dynamics and existence of the monoclinic ferroelectric phase in BiT and BiT like layered materials.

The experiments were performed on highly textured (00l) oriented BiT ceramics (see supplemental material (SM) for details). To confirm phase formation and texture, the X-ray powder diffraction (XRD) spectra were recorded at room temperature (RT) by using a Philips Xpert Pro x-ray diffractometer (Almelo, The Netherlands), as shown in Fig. S-1. For PDF analysis, high resolution powder x-ray diffraction data was recorded using beamline 11-BM at Argonne National Laboratory. The surface morphology of sintered samples was observed using a LEO Zeiss 1550 (Zeiss, Munich, Germany) scanning electron microscope. Transmission electron microscopy was performed using the FEI Titan 300 electron microscope. The THz frequency-domain spectrometer employs a commercial Vector Network Analyzer from Agilent, the N5225A PNA which covered the frequency range from 10 MHz to 50 GHz, and THz frequency extenders as well as matched harmonic detectors developed by Virginia Diodes, Inc. with frequency range from 60 GHz to 1.12 THz. The dynamic range of the instrument reaches 10^{13} with a spectral resolution of less than 100 Hz (see SM).

Fig. 1a shows a bright field cross-section TEM image of textured BiT samples. The cross-section morphology indicates that the plate type BiT grains are stacked along the thickness of the sample confirming the textured microstructure of the BiT. From these images the size of the plate-type grains is in the range of 5–15 μm (Fig. S-2 in SM). The thickness of these plate type grains

was found to be in the range of 200–500 nm (Fig. 1a). The stacking of the pseudo-perovskite and $(\text{Bi}_2\text{O}_2)^{2+}$ layers was clearly observed in the HR-TEM lattice fringes from [100] zone axis, as shown in Fig. 1b. The upper inset in Fig. 1b shows the FFT pattern indicating [100] zone axis, whereas, the lower inset indicates a TEM image with low magnification, revealing layered structure. Due to the two-fold in-plane symmetry, the distinctive stacking of the pseudo-perovskite and $(\text{Bi}_2\text{O}_2)^{2+}$ layers was not observed (Fig. S-2 in SM) from [001] zone axis. The schematic of BiT layered structure at low temperature phase is provided in Fig. 1c.

The high dynamic range and high resolution of our THz frequency-domain spectroscopy allow us to observe the lowest-frequency polar phonon modes or soft phonon modes in BiT materials. The absorption $\alpha(\nu)$ and refractive index $n(\nu)$ of the BiT sample are determined through THz measurements, as shown in Figs. 2a and 2b, respectively for several temperatures. From the absorption and refractive index measurements, we have determined the dielectric response of the sample. The frequency-dependent complex dielectric response, $\epsilon^*(\nu) = \epsilon'(\nu) - i\epsilon''(\nu)$, is related to the complex refractive index, $n^*(\nu) = n(\nu) - i\kappa(\nu)$, through the relations:

$$\begin{aligned}\epsilon'_{\text{sol}}(\nu) &= n^2(\nu) - \kappa^2(\nu) = n^2(\nu) - (c\alpha(\nu)/4\pi\nu)^2 \\ \epsilon''_{\text{sol}}(\nu) &= 2n(\nu) \cdot \kappa(\nu) = 2n(\nu)c\alpha(\nu)/4\pi\nu\end{aligned}\quad (1)$$

where ν is the frequency of the THz radiation. The real part, $n(\nu)$, is the refractive index and the imaginary part, $\kappa(\nu)$, is the extinction coefficient and indicates the attenuation when the radiation propagates through the material. The extinction coefficient, $\kappa(\nu)$, is related to the absorption coefficient through a relation: $\alpha(\nu) = \frac{4\pi \cdot \nu \kappa(\nu)}{c}$, where c is the speed of light.

Figs. 2c and 2d show the permittivity and dielectric loss as a function of THz frequencies at various temperatures, respectively. Unlike the previous report where only one mode was reported at 0.83 THz [7][4], we have observed three polar phonon modes at 0.61 THz (20.35 cm^{-1}), 0.83

THz (27.69 cm^{-1}) and 0.95 THz (31.69 cm^{-1}) at room temperature for the 30 μm BiT sample. Upon heating these components soften and increase their damping.

To gain better insight, the complex dielectric response obtained from our THz frequency-domain spectroscopy for various temperatures were fitted with a sum of three damped Lorentz oscillators describing the optical phonons of the ferroelectric materials [15]:

$$\varepsilon^*(\nu) = \varepsilon_\infty + \sum_{j=1}^3 \frac{A_j/(2\pi)^2}{\nu_j^2 - \nu^2 + i\nu\gamma_j} \quad (2)$$

where $A_j/(2\pi)^2$, ν_j , and γ_j are, respectively, the spectral amplitude of the j damped resonances, its frequency, and its damping coefficient, ε_∞ describes contributions to the dielectric function from modes at frequencies much greater than our experimental range. Three oscillators were employed to the experimental fit of BiT dielectric response spectra related to the three polar phonon modes that are clearly observed in the dielectric response of the BiT film. The temperature dependences of the fit parameters are summarized in Fig. 2e, 2f, and 2g. One can clearly observe the decrease in the frequency of ν_2 and ν_3 with increasing the sample temperature. However, phonon damping was found to increase with temperature for these two modes. Mode ν_1 did not show appreciable changes in frequency and phonon damping. On the other hand, the spectral amplitude of mode ν_1 and ν_3 was found to increase with the increase of the sample temperature as opposed to mode ν_2 . The changes in the amplitude of the modes suggests their couplings with the higher frequency modes of the same symmetry.

In order to understand the relation of these phonon dynamics to Bi–O bonds, atomic PDF analysis was performed at different temperatures. The PDF measurements obtained from a total scattering XRD pattern via a Fourier transform provides us an approach to study the local structure of materials. Because the total scattering pattern is composed of Bragg as well as diffuse scattering

contributions, the information contains local, medium range and long range structure information. The high energy XRD results were corrected for the sample absorption, background, Compton scattering, and incident flux. The intensities were normalized and reduced to the structure factor $S(Q)$ (where Q is the diffraction wave vector), which was Fourier transformed to the corresponding PDFs using PDFgetX[16], $G(r)$ (Fig. S-3 in SM). The $G(r)$ gives the probability of finding a pair of atoms at a distance r [17]:

$$G(r) = \frac{2}{\pi} \int_0^{\infty} Q[S(Q) - 1] \sin(Qr) dQ \quad (3)$$

Having the experimental PDF, one usually wants to determine local structural changes. The PDF results were fitted with B2cb structure having lattice parameters $a = 5.448 \text{ \AA}$, $b = 5.411 \text{ \AA}$, $c = 32.83 \text{ \AA}$, as shown in Fig. 3a. The atomic positions were same as given by Rae et al.[18]. The peaks for the nearest neighbors are highlighted in Fig. 3b. The inset of Fig. 3b shows the experimental PDF, $G(r)$, for BiT at different conditions. One can clearly see the broadening of the peaks related to the bismuth oxide layer and perovskite layer (Fig. 3b). This broadening of the peaks indicates increasing disorder in bismuth layers. Most notably, the peak related to the perovskite layer is not just broadened, but also, became asymmetric indicating increased anharmonicity of the Bi–O bonds. The anharmonicity of these bonds plays a significant role in the shifting of the soft phonon modes, and thereby, in the structural phase transitions.

In order to gain further insights into the experimentally observed phonon dynamics and bond anharmonicity, the three soft phonon modes were analyzed using the atomic forces derived from DFT [19,20]. The generalized gradient approximation (GGA) [21] was used as the exchange-correlation functional together with the projector-augmented wave method as implemented in the Vienna *ab initio* Simulation Package (VASP) [22-24]. The primitive cell dimensions for the low

temperature phase ($T < 600$ °C) of BiT with space group Pc were found to be $a = 5.49$ Å, $b = 5.53$ Å, $c = 16.88$ Å, and $\alpha = 80.61^\circ$. These values are in good agreement with experimental reports [25] and other first-principles computations [26]. Phonon calculations were performed by linear response method [27] and also by the frozen phonon method as implemented in Phonopy [28] (see SM). Phonopy is used to extrapolate the DFT results (condition similar to absolute zero temperature) to finite temperatures using a quasi-harmonic approximation[28]. Combination of DFT with frozen phonon method provides the platform to analyze lattice dynamics, soft modes, and phase transformations.

The phonon density of states (DOS) obtained for temperature -273 °C, 127 °C, and 527 °C from Phonopy are shown in Fig. 4. Out of the several peaks that are observed, our focus is on the lowest three phonon modes with frequencies 1.13 THz, 1.14 THz, and 1.37 THz, as obtained from the linear response method. These are contained in the first peak shown in Fig. 4. We observed that the DOS shifts to lower frequencies with increasing temperature. The three low frequency phonons shift by 7.1%, 2.6% and 1.3%, respectively, from -273 °C to 527 °C. The corresponding displacement of phonon frequencies for hydrostatic expansion of the lattice by 1% is found to be 12.9%, 5.3% and 2.6%, providing the clue that the phonon softening is also associated with the volume expansion of the lattice together with the anharmonicity of the Bi–O bonds.

The phonon modes for the lowest three frequencies are shown in SM (animated gif files) where the vibration of ions in the perovskite- and fluorite-blocks are displayed. The correlated motion of atoms within each block, which are out-of-phase among each other, is shown in the gray and green regions in Fig. 1c. The main contribution to the atom-projected phonon DOS (inset of Fig. 4) comes from Bi atoms, and a small percentage comes from O atoms. It is thus inferred that the out-of-phase oscillations of the lattice blocks together with the temperature dependent volume

expansion are the reasons for the monoclinic to tetragonal phase change (Fig. 1*d*). As described in Fig. 1*e*, the structural change is associated with monoclinic lattice parameter transformation $a < b \rightarrow a' = b'$, such that the lattice parameter of the tetragonal phase is $a' (=b') = a\sqrt{2}$. This mechanism is consistent with the theoretical findings of Ref. [29], where it is suggested that two unstable E_u modes in BiT, one involving the motion of fluorite layers in a direction relative to the perovskite $(\text{TiO}_6)^{8-}$ blocks and the second mode involving the motion of the Bi ions in the perovskite A site with respect to the perovskite blocks, are responsible for the phase change. The atomic displacements in the fluorite layers are larger than in the perovskite layers for the three calculated modes in our study. Thus, the chemical nature of large cation in the fluorite layers in the Aurivillius family and similar layered oxides can be crucial in phase transitions behavior.

In summary, we have probed dynamics of soft phonon modes and its role in the phase transitions on highly textured (001) oriented $\text{Bi}_4\text{Ti}_3\text{O}_{12}$ using the THz frequency-domain spectroscopy. The results from the THz frequency-domain spectroscopy have revealed three low frequency phonon modes related to the phase transitions in BiT material from low temperature monoclinic to high temperature tetragonal phase. Our results underline the facts that the anharmonicity of the Bi–O bonds and volume expansion of lattice play a leading role in softening the low frequency phonons. The majority contribution to the phonon density of states of low frequency modes was from Bi atoms, followed by O atoms. The displacements of Bi atoms in fluorite layers are larger than in the perovskite layers. The results provide the hint for fabricating the materials in order to achieve the desired critical temperature for practical ferroelectric devices.

Acknowledgment: This work was supported by the AFOSR through grant FA9550-14-1-0376. The terahertz-dielectric study was supported by the Institute of Critical Technology and Applied Sciences (ICTAS) at Virginia Tech. MGK and HCS acknowledge financial support through the Department of Energy program (DE-FG02-09ER46674). The computational resources from the Taylor L. Booth Engineering Center for Advanced Technology (BECAT) at University of Connecticut and Extreme Science and Engineering Discovery Environment (XSEDE), which is supported by National Science Foundation

grant number ACI-1053575, are gratefully acknowledged. One of the authors (F.-C. S) would like to thank J. Skelton at University of Bath and H. Tran and K. Pitike at University of Connecticut for helpful discussions. Use of the Advanced Photon Source at Argonne National Laboratory was supported by the U. S. Department of Energy, Office of Science, Office of Basic Energy Sciences, under Contract No. DE-AC02-06CH11357. F.-C. S and D. G. contributed equally to this work.

References

- [1] J. Hlinka, T. Ostapchuk, D. Nuzhnyy, J. Petzelt, P. Kuzel, C. Kadlec, P. Vanek, I. Ponomareva, and L. Bellaiche, *Physical Review Letters* **101**, 167402 (2008).
- [2] D. Wang, A. A. Bokov, Z. G. Ye, J. Hlinka, and L. Bellaiche, *Nat Commun* **7** (2016).
- [3] M. S. Senn, D. A. Keen, T. C. A. Lucas, J. A. Hriljac, and A. L. Goodwin, *Physical Review Letters* **116**, 207602 (2016).
- [4] D. Nuzhnyy *et al.*, *Phys Rev B* **74** (2006).
- [5] J. M. Perez-Mato, P. Blaha, K. Schwarz, M. Aroyo, D. Orobengoa, I. Etxebarria, and A. García, *Phys Rev B* **77**, 184104 (2008).
- [6] W. S. Choi and H. N. Lee, *Phys Rev B* **91**, 174101 (2015).
- [7] B. H. Park, B. S. Kang, S. D. Bu, T. W. Noh, J. Lee, and W. Jo, *Nature* **401**, 682 (1999).
- [8] C. Chiritescu, D. G. Cahill, N. Nguyen, D. Johnson, A. Bodapati, P. Keblinski, and P. Zschack, *Science* **315**, 351 (2007).
- [9] E. J. Nichols, J. W. J. Shi, A. Huq, S. C. Vogel, and S. T. Mixture, *J Solid State Chem* **197**, 475 (2013).
- [10] J. H. Lee, R. H. Shin, and W. Jo, *Phys Rev B* **84**, 094112 (2011).
- [11] A. Shrinagar, A. Garg, R. Prasad, and S. Auluck, *Acta Crystallogr A* **64**, 368 (2008).
- [12] M. Iwata, K. Ando, M. Maeda, and Y. Ishibashi, *Journal of the Physical Society of Japan* **82**, 025001 (2013).
- [13] M. Kempa, P. Kuzel, S. Kamba, P. Samoukhina, J. Petzelt, A. Garg, and Z. H. Barber, *J Phys-Condens Mat* **15**, 8095 (2003).
- [14] D. K. George, A. Charkhesht, and N. Q. Vinh, *Review of Scientific Instruments* **86**, 123105 (2015).
- [15] N. Q. Vinh, M. S. Sherwin, S. J. Allen, D. K. George, A. J. Rahmani, and K. W. Plaxco, *The Journal of Chemical Physics* **142**, 164502 (2015).
- [16] P. Juhas, T. Davis, C. L. Farrow, and S. J. L. Billinge, *Journal of Applied Crystallography* **46**, 560 (2013).
- [17] Y. Yasuhiro, K. Shinji, and M. Jun'ichiro, *Japanese Journal of Applied Physics* **45**, 7556 (2006).
- [18] A. D. Rae, J. G. Thompson, R. L. Withers, and A. C. Willis, *Acta Crystallographica Section B* **46**, 474 (1990).
- [19] W. Kohn and L. J. Sham, *Physical Review* **140**, A1133 (1965).
- [20] P. Hohenberg and W. Kohn, *Physical Review* **136**, B864 (1964).
- [21] J. P. Perdew, K. Burke, and M. Ernzerhof, *Physical Review Letters* **77**, 3865 (1996).
- [22] G. Kresse and D. Joubert, *Phys Rev B* **59**, 1758 (1999).
- [23] G. Kresse and J. Furthmüller, *Computational Materials Science* **6**, 15 (1996).
- [24] G. Kresse and J. Furthmüller, *Phys Rev B* **54**, 11169 (1996).
- [25] J. Min Ku, K. Yong-II, N. Seung-Hoon, S. Jung Min, J. Chang Hwa, and W. Seong Ihl, *Journal of Physics D: Applied Physics* **40**, 4647 (2007).
- [26] D. J. Singh, S. S. A. Seo, and H. N. Lee, *Phys Rev B* **82**, 180103 (2010).
- [27] S. Baroni and R. Resta, *Phys Rev B* **33**, 7017 (1986).
- [28] A. Togo and I. Tanaka, *Scripta Materialia* **108**, 1 (2015).
- [29] R. Machado, M. G. Stachiotti, R. L. Migoni, and A. H. Tera, *Phys Rev B* **70**, 214112 (2004).

Figures

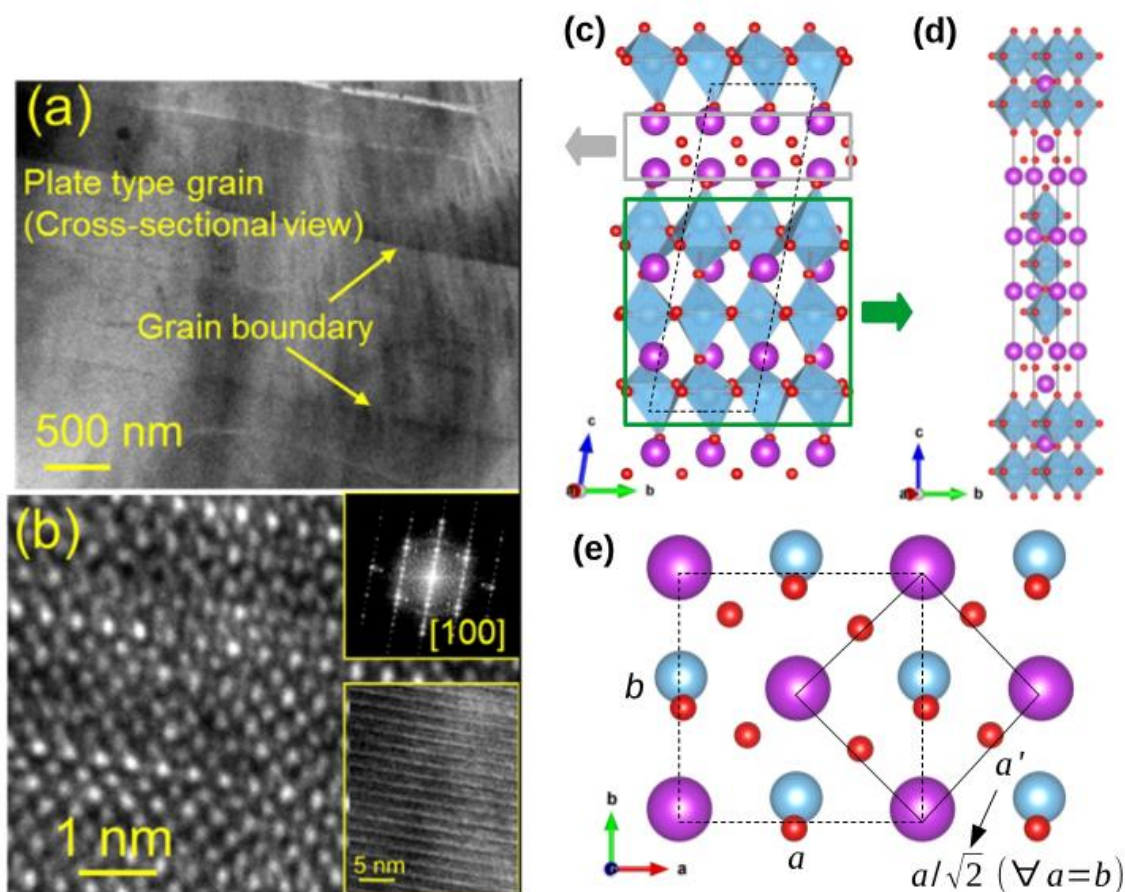


Figure-1 (a) Bright field cross-section TEM image of plate type grains of BiT demonstrate the thickness of these plate type grains in the range of 200–500 nm. (b) The HR-TEM lattice fringe images of BiT ceramics observed from zone axis [100] indicate the stacking of the pseudo-perovskite and $(\text{Bi}_2\text{O}_2)^{2+}$ layers. The lower inset of (b) shows the corresponding low magnification image. Note the images of Bi_2O_3 layers in a HR-TEM image are collected with the electron beam parallel to the [100] zone axis. The upper inset of (b) depicts the corresponding FFT patterns indicating [100] zone axis. Low and high temperature phases of the relaxed BiT structures are shown in (c) and (d), respectively. Bi is denoted by large purple spheres, O by small red spheres. Ti ions stay at the center of the light blue octahedra surrounding by six O atoms. (e) The suggested transformation path from monoclinic to tetragonal phases. This transition is associated with the opposite movement of the fluorite- and perovskite-like layers, indicated by gray and green arrows shown in (c), respectively.

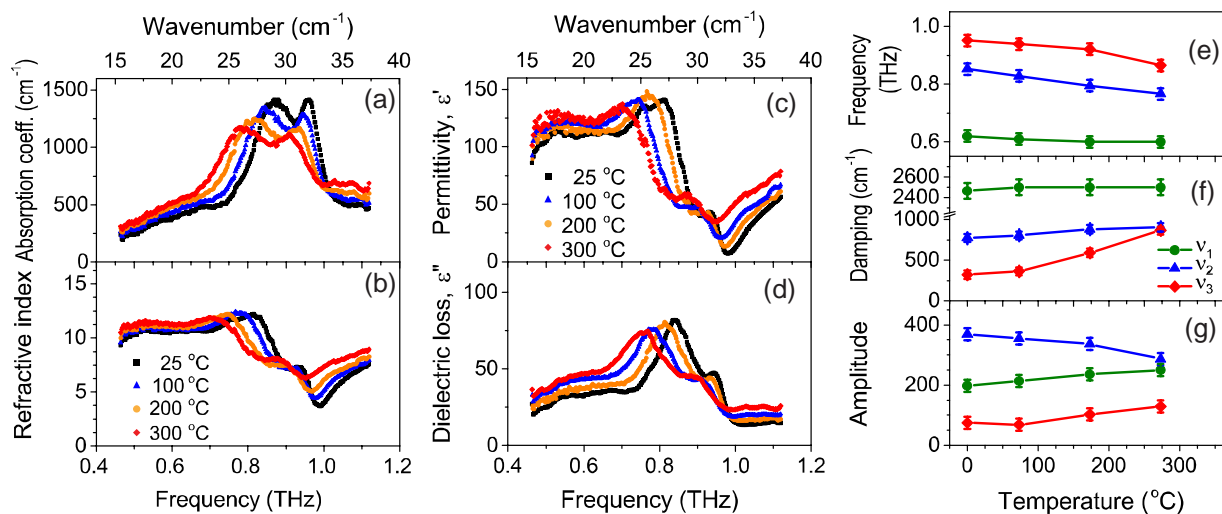


Figure 2: The terahertz (a) absorption and (b) refractive index of the *c*-oriented textured polycrystalline BiT ceramic material were recorded at various temperatures. Complex terahertz dielectric response including (c) the permittivity and (d) the dielectric loss at different temperatures calculated from their absorption and refractive index provides insight into the dynamics structure of the BiT material. Complex terahertz dielectric response measurements show temperature dependence of (e) lowest soft phonon frequencies ν_1 , ν_2 and ν_3 , (f) phonon damping γ_1 , γ_2 , γ_3 and (g) their amplitudes.

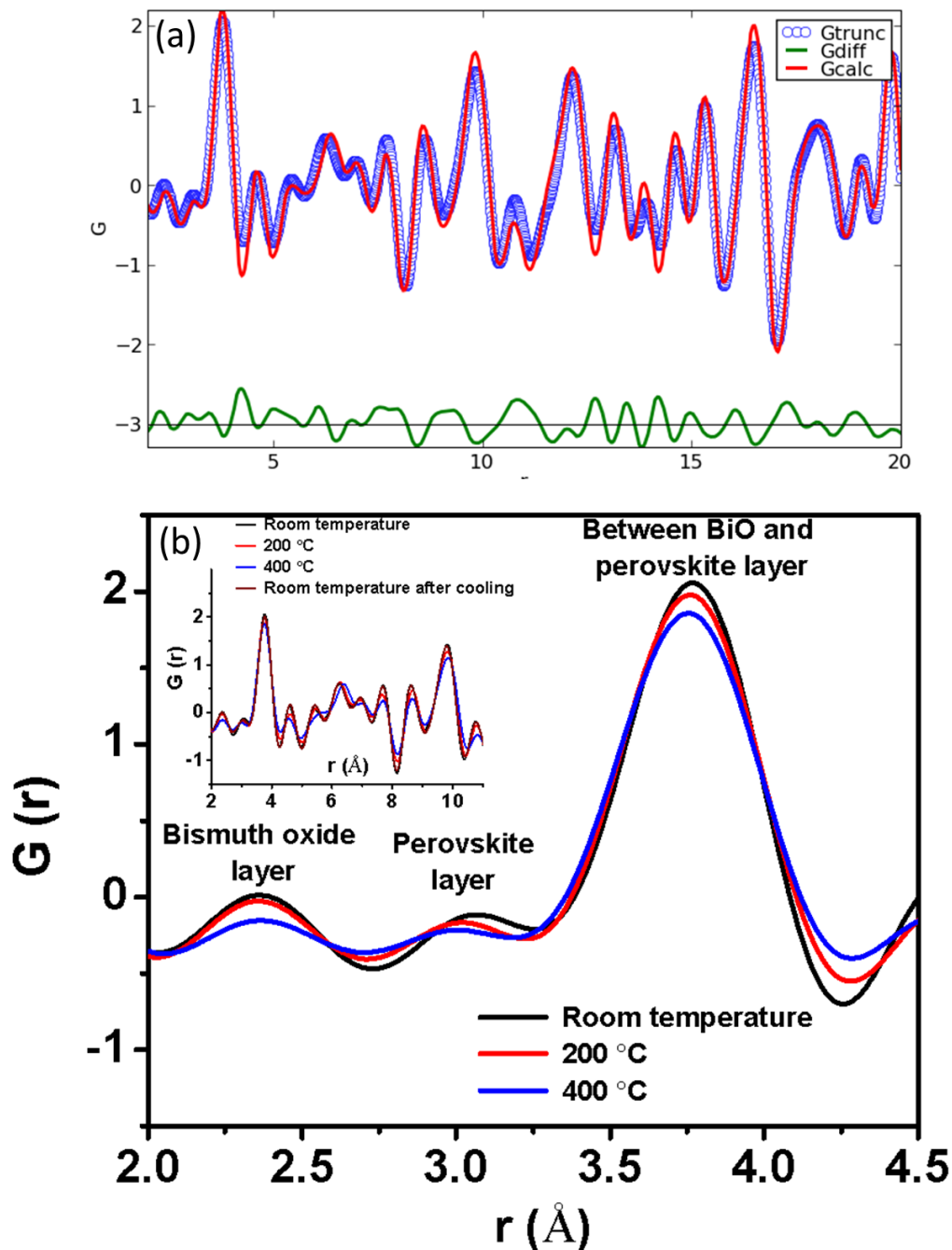


Figure 3: (a) The fit obtained using PDFGUI for B2cb structure in BIT. (b) Peaks indicate the closest neighbor Bi-O bonds. The Bi-O bonds show significant disordered structure at higher temperatures for both bismuth oxide and the perovskite layers. The inset of Fig. 3(b) show the pair distribution functions, $G(r)$, measured under different conditions, providing a relation between the dynamics of Bi ions with phonon dynamics. The calculated pattern for the B2cb structure (high temperature orthorhombic phase) is shown with dotted line.

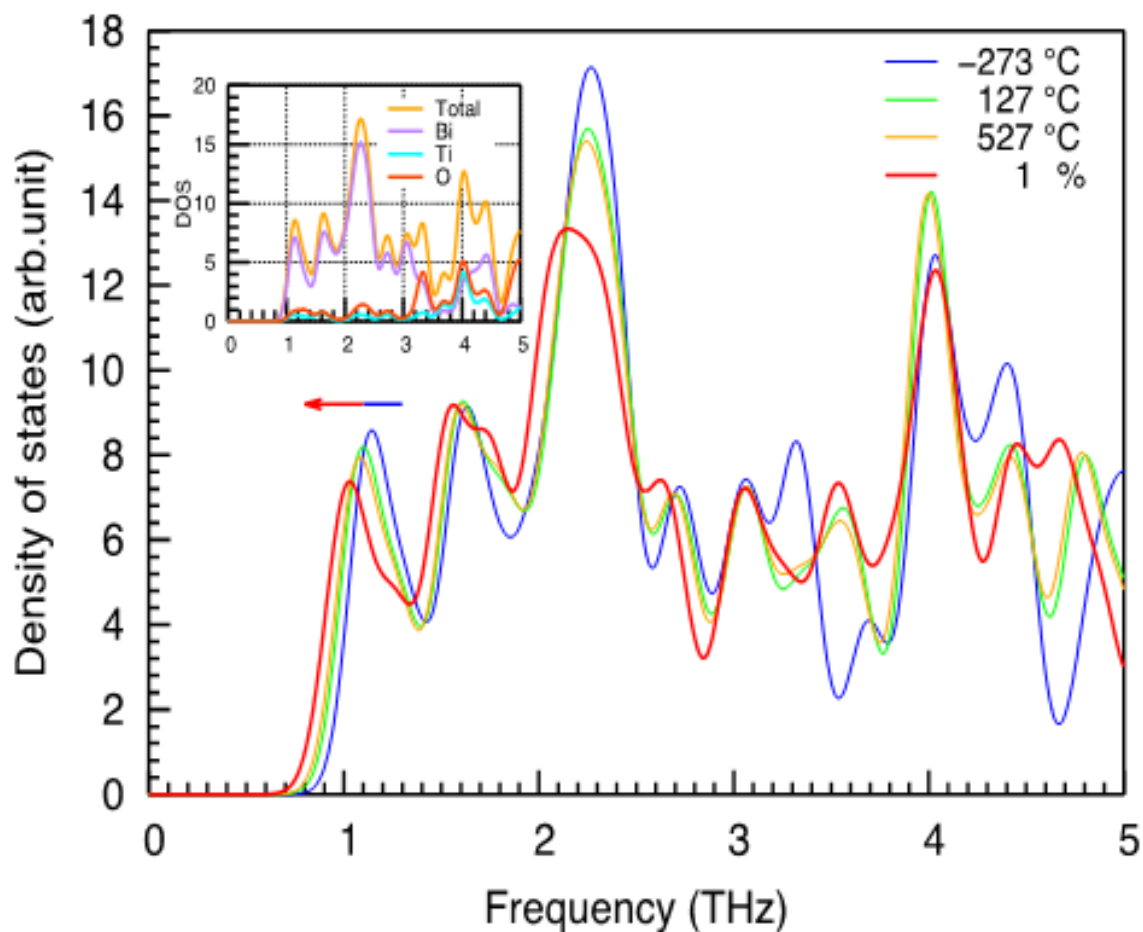


Figure 4: Phonon density of states (DOS) calculated using frozen phonon approximation to the dynamical matrix using *Phonopy*. The quasi-harmonic approximation is used for extrapolation to finite temperature. The peaks shift to lower frequency with increasing temperature. The result for a 1% volume expansion is also shown for comparison. The inset shows atomic contribution to the total phonon DOS, suggesting that a major contribution to phonons in the low frequency range is due to the Bi atoms.

Supplemental material:

Soft Phonon Mode Dynamics and Phase Transitions in Aurivillius Type Structures

Deepam Maurya¹, Fu-Chang Sun², Deepu George³, Sanjeev K. Nayak², Abhijit Pramanick, Min-Gyu Kang¹, Hyun –Cheol Song¹, Ali Charkhesht³, S. Pamir Alpay², Giti A. Khodaparast³, N. Q. Vinh³, and Shashank Priya¹

¹*Bio-inspired Materials and Devices Laboratory (BMDL), Center for Energy Harvesting Materials and Systems (CEHMS), Virginia Tech, 24061 USA*

²*Department of Materials Science & Engineering, Department of Physics, Institute of Materials Science, University of Connecticut, Storrs, CT 06269-3136, USA*

³*Department of Physics, Virginia Tech, 24061 USA*

⁴*Department of Physics and Materials Science, City University of Hong Kong, Kowloon, Hong Kong SAR*

1. Sample preparation:

In order to synthesize textured Bi₄Ti₃O₁₂ (BIT) ceramics, first BIT platelets were synthesized using molten salt synthesis method.[1] For this, stoichiometric amount of Bi₂O₃ and TiO₂ ceramics were ball milled for 24h under ethyl alcohol in polyethylene bottle with yttria-stabilized zirconia (YSZ) balls as milling media. This slurry was further dried in an oven at 60°C for 6 h. The resulting powder was mixed with equal amount of salt mixture (56wt% KCl and 44wt% NaCl) and heated at 1150°C for 30 min. Next, this product was washed several times in deionized water to remove salt and realize BIT platelets. These platelets were pressed to fabricate cylindrical pellets which were sintered at 1150°C for 2h. Furthermore, during high temperature processing, all the specimens were muffled with the powder of the same composition in order to maintain the chemical composition. During pressing, the anisotropic BIT particles with large aspect ratio were aligned with the major surface perpendicular to the pressing direction, which resulted in textured BIT ceramics after sintering.

2. Texture and microstructure

Room temperature XRD-spectra were recorded by using a Philips Xpert Pro x-ray diffractometer (Almelo, The Netherlands). These XRD patterns clearly suggest formation of pure BIT phase. The change in the intensity of Bragg reflections in the XRD-spectrum of textured BIT clearly suggests high degree of texturing. The degree of orientation was determined from the XRD pattern of the textured BIT in the range of $2\theta = 10 - 50^\circ$ by Lotgering's method. The Lotgering factor f is defined as the fraction of area textured with required crystallographic plane using the formula:[2]

$$\text{Lotgering Factor } f_{00l} = \frac{P - P_o}{1 - P_o}, P = \frac{\sum I(00l)}{\sum I(hkl)}, P_o = \frac{\sum I_o(00l)}{\sum I_o(hkl)} \quad (1)$$

where I and I_o are intensity of the diffraction lines (hkl) of textured and randomly oriented specimens, respectively. The degree of texturing (calculated using Lotgering factor) was found to be 96% suggesting sintered ceramics are highly oriented along c -axis.

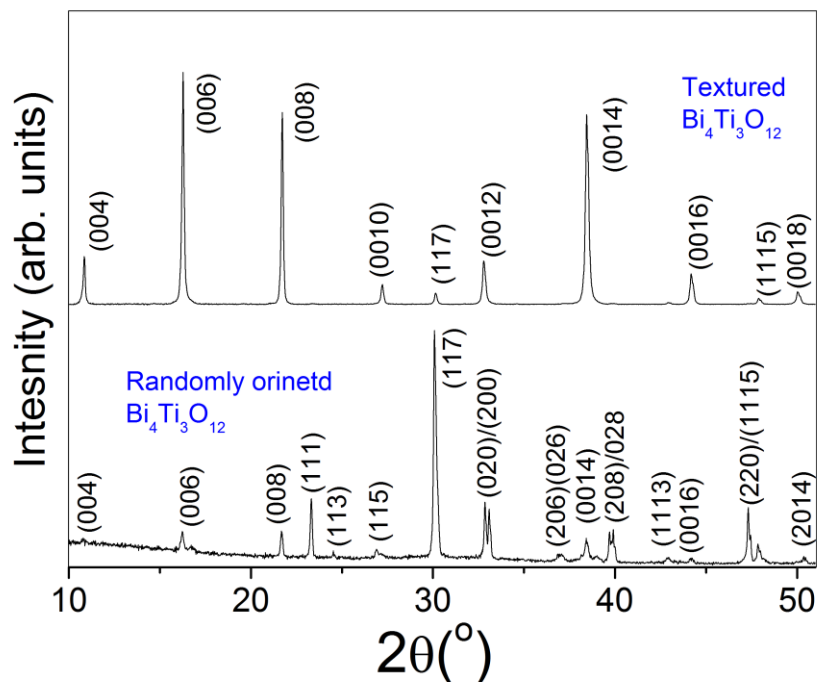


Fig. S-1 XRD –spectra recorded RT for textured and randomly oriented BIT ceramics. Please note the change in the intensity of textured BIT ceramics indicating high degree of the crystallographic orientation along c -axis.

The surface morphology of the sintered samples was observed using a LEO Zeiss 1550 (Zeiss, Munich, Germany) scanning electron microscope. In order to prepare the electron transparent TEM specimens, we used standard grinding and ion-milling method. For conducting transmission electron microscopy, we used a FEI Titan 300 microscope.

Fig.S-1 shows XRD-patterns recorded at room temperature for textured BIT ceramics. The change in the intensity of various Bragg reflections compared to randomly oriented counterpart, suggests a high degree of texture along c -axis. The lotgering factor f_{00l} calculated from these XRD-patterns suggested 96% texturing in $\langle 001 \rangle$ orientation. In order to investigate morphology of the textured BIT samples, SEM micrographs were recorded on the flat surface (Fig. S-2a). The flat surface clearly shows a plate type (major surface in the plane of the sample's top surface) grain morphology. The cross-section morphology indicates that the plate type BIT grains are stacked along the thickness of the sample. This morphology confirms the textured microstructure of BIT. From these images it can be seen that the size of the plate-type grains was in the range of 5-15 μm . The thickness of these plate type grains was found to be in the range of 200-500nm (Fig. S-2(a)). Fig S-2(b) and S-2(c) show the bright field cross-section TEM micrographs of a plane view samples. The grain boundaries in textured BIT are the result of fusing BIT plates together (during high temperature sintering process) mostly with a slight miss-orientation. Fig. S-2(d) show a HR-TEM image of the lattice fringes from $[001]$ orientation. Due to the twofold in-plane symmetry, the distinctive stacking of the pseudo-perovskite and $(\text{Bi}_2\text{O}_2)^{2+}$ layers was not observed. Moreover, the layered structure of these materials was found to be useful in decreasing the thermal conductivity due to effective phonon scattering.[3]

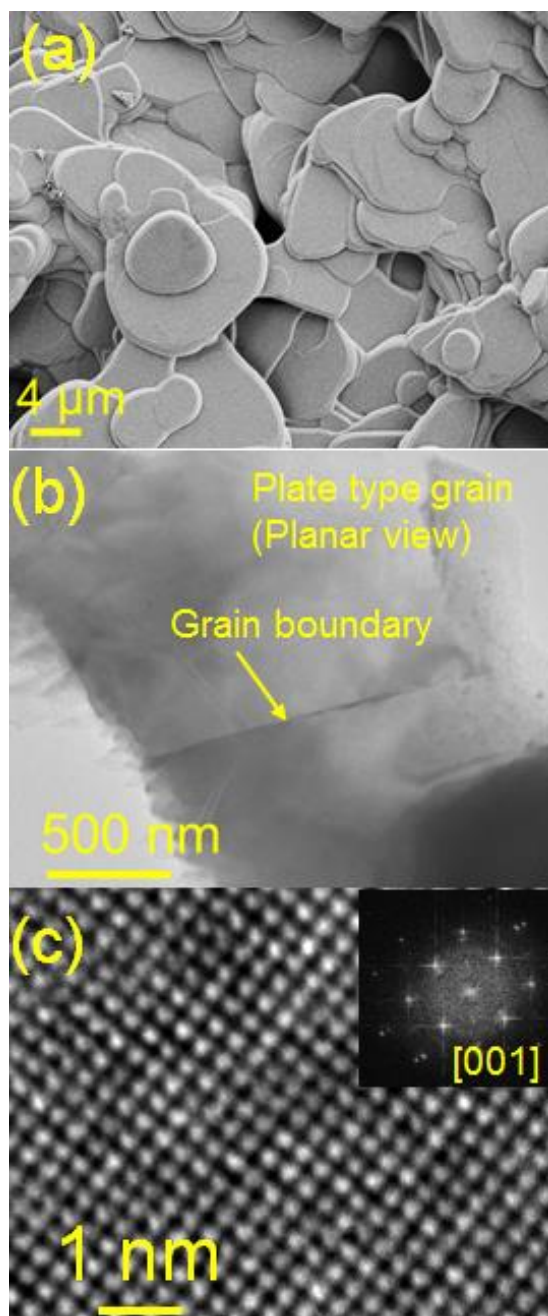


Fig.-S-2 (a) SEM micrographs of $\langle 001 \rangle$ textured BIT from top surface. (b) Bright field TEM image of the plate type grains from the top surface. (c) The HR-TEM lattice fringe images of BIT ceramics from $[001]$ zone axis. The inset of (c) shows FFT patterns marked with the zone axes.

3. Terahertz (THz) measurements:

The details of THz spectrometer measurements can be found elsewhere[4]. The spectrometer supports the simultaneous measurements of absorbance and refractive index of solutions over the

spectral range from 26.5 GHz to 1.12 THz (0.88 to 37.36 cm^{-1} or 0.268 to 11.3 mm). The signal-to-noise and spectral resolution of this device were significantly high as compared to any previous state-of-the-art instruments. For example, while the dynamic range of a commercial terahertz time-domain spectrometer is just 10^6 and its spectral resolution is several gigahertz, the dynamic range of our instrument reaches an unprecedented value of 10^{13} and the system achieves a spectral resolution of less than 100 Hz.[4-6] The system provides a coherent radiation source with a power up to 20 mW in the gigahertz-to-terahertz region.

For transmission measurements, we employed a quasi-optical setup. The transmitter module emits terahertz radiation into free space with a circular horn. The radiation transmitted through the sample is subsequently collected using a similar horn and is fed into a receiver module. For temperature dependent measurements, we used a home built temperature controlled setup made of a large aluminum block and high power resistances. Temperature of the sample was controlled with an accuracy of ± 2 °C by varying the voltage applied to the power resistances. The BIT film was placed on a brass sample holder using thermal paste and was attached to an aperture on the setup. An identical aperture and empty sample holder formed reference signals. The translation stage allowed alternative reference and sample measurements under identical conditions. The high dynamic range combined with the ability to detect the phase allowed an accurate measurements of absorption coefficient and refractive index of highly absorptive samples like BIT. The experiment consists of two consecutive measurements for each temperature: (i) Measurements of the reference signals of transmitted intensity and phase shift with an empty sample holder. (ii) Measurements of intensity and phase shift after the BIT sample.

4. Atomic Pair Distribution Function (PDF) results:

The atomic pair distribution function analysis can be used to understand local structural changes. PDFgetX was used to compute $G(r)$ from the X-ray diffraction data recorded on $\text{Bi}_4\text{Ti}_3\text{O}_{12}$, as shown in Fig. S-3. The Q_{maxinst} was limited to 10 \AA^{-1} due to the increased noise. The wavelength used for calculations is 0.414211 \AA .

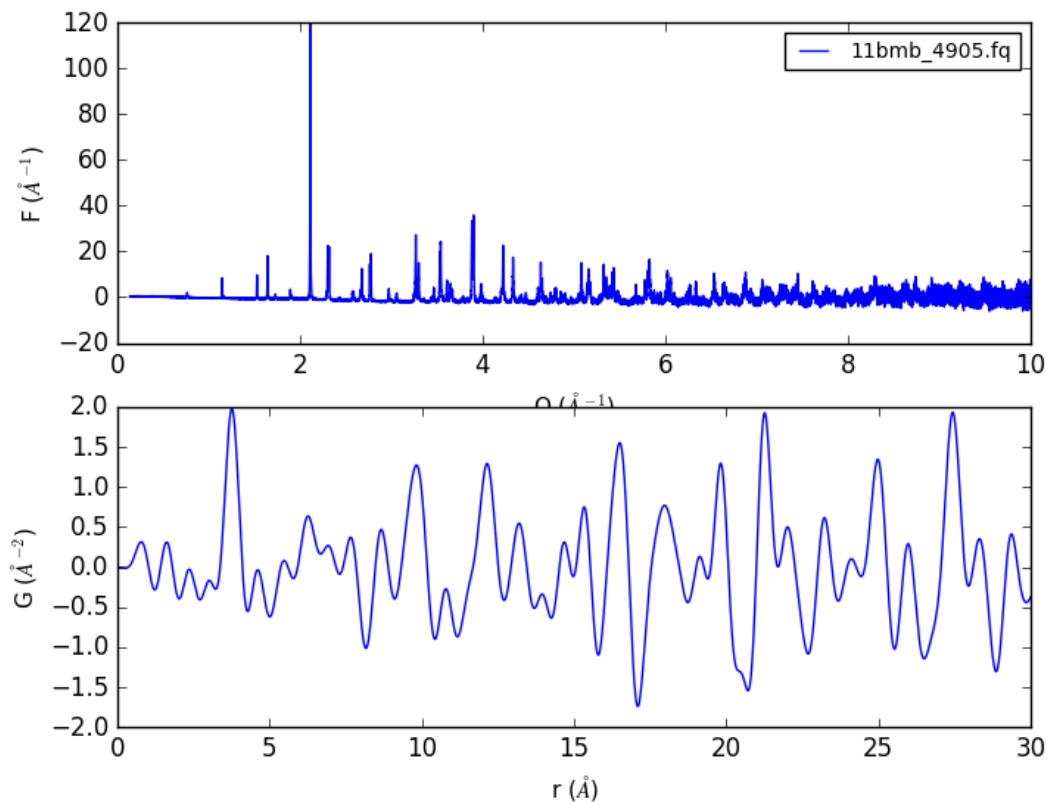


Fig. S-3: $F(Q)$ and $G(r)$ profiles for BIT from PDFgetX. [7]

5. Density functional theory based calculations

We carried out first-principles calculations using density functional theory (DFT) as implemented in the Vienna *ab initio* Simulation Package (VASP). The generalized gradient approximation (GGA) parameterized by Perdew-Burke-Ernzerhof was used for the exchange correlation functional together with the projector augmented wave method. The \mathbf{k} -point mesh was

taken as $8 \times 8 \times 2$ with Γ centered Monkhorst-Pack grids, along with the plane wave energy cutoff 500 eV. The energy tolerance for self-consistent field calculations was set to 10^{-6} eV. The lattice parameters were found to be $a = 5.49 \text{ \AA}$, $b = 5.53 \text{ \AA}$, $c = 16.88 \text{ \AA}$, and $\alpha = 80.61^\circ$ for the minimum energy crystal structure in space group Pc . In this study, we implemented the frozen phonon method to construct the dynamical matrix for phonon frequency calculations using Phonopy. By quasi-harmonic approximation, where the change of the volume is considered as the effect by thermal expansion, the finite displacement calculations were performed at a series of unit cell within approximately $\pm 6\%$ of the equilibrium volume. The equilibrium states at each finite lattice temperature were determined by fitting to the Murnaghan's equation of state. These relaxed structures of the unit cell were expanded to $2 \times 2 \times 2$ supercell to compute the phonon density of states (DOS). The volume corresponding to temperature at 0 K, 400 K, and 800 K were selected and compared with the experimental findings.

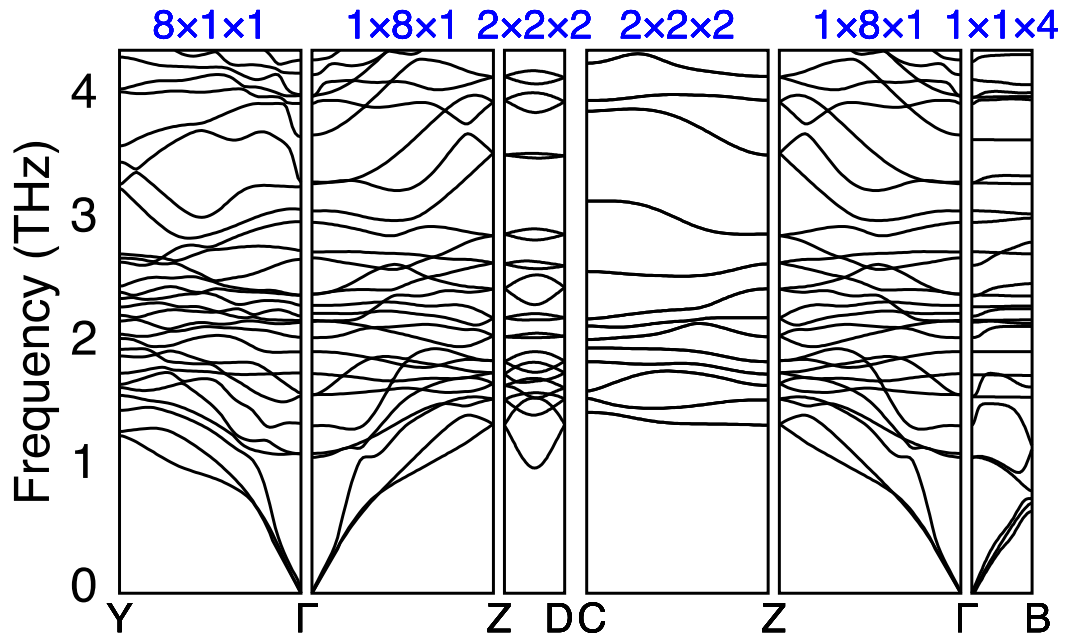


Fig. S-4: Phonon band structure for the monoclinic BIT lattice. The appropriate size of supercell is chosen as shown in the top panel to incorporate the commensurate points along the path between high symmetry points.

The phonon band diagram was established by appropriately expanding the size of the supercell to account for all the commensurate points along x - (Γ -Y), y - (Γ -Z), and z -axes (Γ -B), as shown in Fig. S-4. This was found to be in the same direction of lattice parameters, a , b , and c , respectively. To determine the complete band diagram, computationally feasible supercells of size up to $8 \times 8 \times 4$ consisting of 9728 atoms are required which is not computational feasible. In the animated gif files, the vibration of ions in the perovskite- and fluorite-blocks were displayed. The Screenshot of these animated gif files showing the phonon modes for the lowest three frequencies is depicted in Fig. S-5.

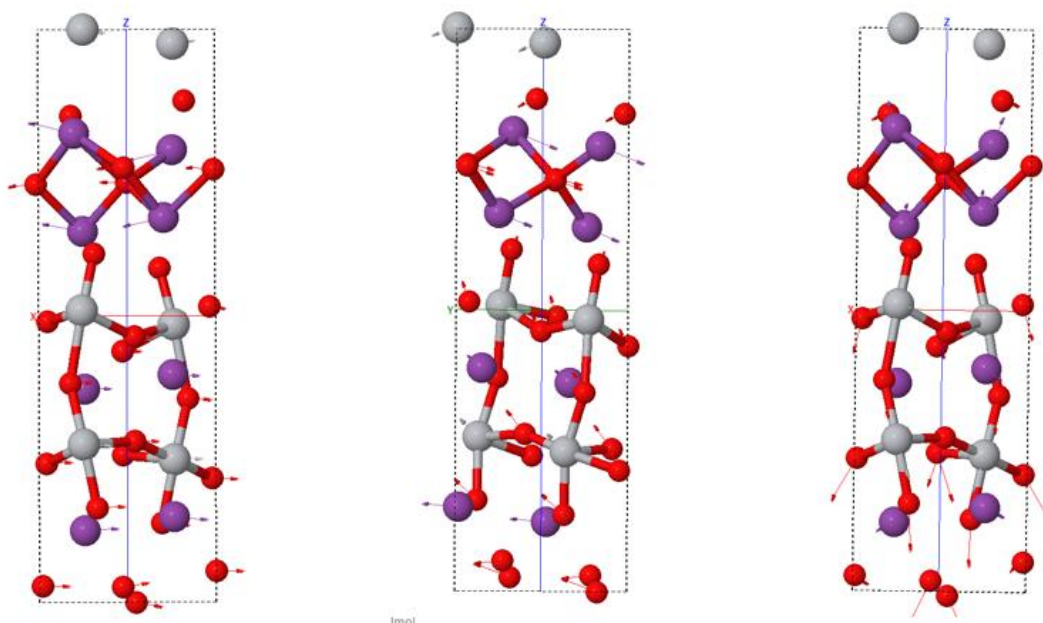


Fig. S-5 Screenshot of the animated gif files of the lowest frequency vibration modes depicting the phonon modes for the lowest three frequencies.

References:

- [1] D. Maurya, Y. Zhou, Y. Yan, and S. Priya, *Journal of Materials Chemistry C* **1**, 2102 (2013).
- [2] F. K. Lotgering, *J Inorg Nucl Chem* **9**, 113 (1959).
- [3] C. Chiritescu, D. G. Cahill, N. Nguyen, D. Johnson, A. Bodapati, P. Keblinski, and P. Zschack, *Science* **315**, 351 (2007).
- [4] D. K. George, A. Charkhesht, and V. N. Q., *Review of Scientific Instruments* **86**, 123105 (2015).
- [5] N. Q. Vinh, S. J. Allen, and K. W. Plaxco, *J Am Chem Soc* **133**, 8942 (2011).
- [6] N. Q. Vinh, M. S. Sherwin, S. J. Allen, D. K. George, A. J. Rahmani, and K. W. Plaxco, *J Chem Phys* **142**, 164502 (2015).
- [7] A. D. Rae, J. G. Thompson, R. L. Withers, and A. C. Willis, *Acta Crystallographica Section B* **46**, 474 (1990).